ORIGINAL RESEARCH

An investigation on temperature-dependant surface properties of porous carbon nanoparticles derived from biomass

S. Supriya[1,2] · Vinay S. Bhat[1] · Titilope John Jayeoye[3] · Thitima Rujiralai[3] · Kwok Feng Chong[4] ·
Gurumurthy Hegde[1,5]

Abstract

In this work, a detailed investigation on the temperature-dependant surface features of biomass derived porous carbon nanoparticles was conducted. The carbon nanoparticles were prepared by carbonization of *Caesalpinia Sappan* waste pods in single step pyrolysis, using a range of temperature from 400 to 1000 °C. The systematic analysis of materials obtained at different temperatures assisted to correlate the effect of pyrolysis temperature on the surface properties. Different methods were employed which were beneficial to demonstrate the overall surface area and porous features constituted by pores of different size (micropores, mesopores) and shapes such as cylindrical or narrow slit shape. This study confirmed the optimization of material properties with rise in pyrolysis temperature; as a result, *Caesalpinia Sappan* derived carbon nanoparticles pyrolyzed at 1000 °C (CSCNP1000) exhibited the largest surface area (794 $m^2 g^{-1}$ by BET) and pore volume (0.37 $cm^3 g^{-1}$) in the series. The resulted carbon products were microporous/mesoporous in nature, the condition which is considered suitable for the energy storage applications. The energy storage device, supercapacitor, was fabricated which exhibited a specific capacitance of 170.5 $F g^{-1}$ at 0.25 $A g^{-1}$. This work demonstrated the suitability of temperature dependent surface of a carbon nanoparticle to be actively used as a cost-effective energy storage device.

✉ Gurumurthy Hegde
   murthyhegde@gmail.com

1   Centre for Nano-Materials and Displays, B.M.S.
    College of Engineering, Bull Temple Road, Bengaluru,
    Karnataka 560019, India

2   Department of Chemistry, B.M.S. College of Engineering,
    Bull Temple Road, Bengaluru, Karnataka 560019, India

3   Division of Physical Science, Faculty of Science, Prince
    of Songkla University, Hat Yai 90112, Songkla, Thailand

4   Faculty of Industrial Sciences and Technology, Universiti
    Malaysia, 26300 Kuantan, Pahang, Malaysia

5   Adindistech Private Limited, B102, Manpho Pavillion
    Building, Bengaluru 560076, India
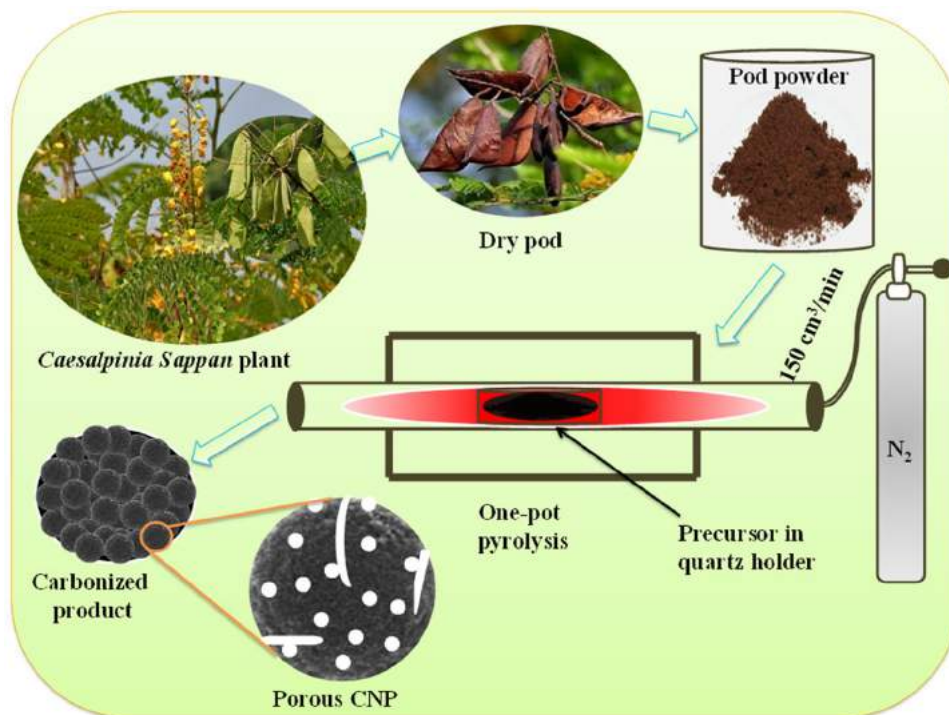
Springer

Graphic abstract

Introduction

Particle size and surface area have been the significant facets which persuade nanoparticles/nanomaterials to manifest unique properties. It has been now understood that one can design and develop a new nano- structure or device by controlling the size, shape and surface features [1]. Therefore, since last few decades, nanoscience and nanotechnology has been crowned as a leading field of science and engineering and integrated with most of the disciplines including physics, chemistry, biology, materials, medicine, space exploration, etc. [2]; it also has enormously become a part of daily life products such as cosmetics, food packaging, sensors, purification agents, etc.

In the materials having high surface area, as in nanoporous materials, the surface properties dominate overall material behaviourr [3]. This allows the architecture of novel nanoscale porous materials, which open new dimensions of designing materials for technological important areas such as energy storage and conversion, photochemical applications, catalysis, sensing and water desalination [4]. In this regard, the molecular design and tailoring of surface properties of porous carbonaceous materials has gained huge attention in recent years [5, 6]. The tuning

of carbon surface has been proven to be a powerful tool to change the surface polarity, electrochemical landscape and wettability [5, 7–12]. Further, the nanoporous carbons, generally, contain pores in a broad range from micro- to macropores [13]. The functions executed by these pores are different [14]; macropores behave as reservoirs of ion for micro and mesopores; mesopores provide adequate channels of transport for the diffusion of ions; and the micropores act as molecular sieves and control the charge status and capacitance of the material by controlling the diffusion of ions. These behaviours of different porous structures are useful for various applications.

The current scenario demands sustainable carbon nanomaterials with large surface area and porosity prepared from an inexpensive carbon source by simple fabrication method, so that they could be utilized in a wide range of industrial/technological applications [15–19]. In this regard, biomass, a natural source of carbon has been widely used to prepare porous carbon nanostructures because of abundant availability [20, 21]. In the past few years, several plant-, animal- and microorganism-based biomasses have been applied for this purpose [22]. The major advantage of biomass as raw material is that it facilitates construction of porous carbon material with high

specific surface area. Another important advantage is that the bio- precursors are rich with heteroatom composition, such as N, O, S, K, etc. which act as natural dopants for porous carbon [23]. Further, the biomass allows transformation to sustainable nanocarbon materials by simple procedures like hydrothermal carbonization, ionothermal carbonization and direct pyrolysis [24].

Generally, the porous carbon nanomaterials prepared from biomass demand physical/chemical activation processes for enhancing the surface features [25–27]; but in the current study, the waste dry pods of *Caesalpinia Sappan* is converted in to spherical shaped porous carbons in nanoscale by one-step pyrolysis method, without using activating agents. *Caesalpinia Sappan* is a leguminous tree that could most commonly be found in India, Thailand, Malaysia, China, and Myanmar. It belongs to family Leguminoesae and is known by different names, such as Biancaea sappan, Sappan wood, False Sandalwood, Brazil wood, Patang, etc. The pods of Sappan tree are woody, indehiscent and obliquely oblong. The pods produce large amount of biomass once the seeds ripe. The chemical composition of pods is constituted by tannin, flavonoids, lignin, vitamins, and metal contents [28]. The hard wood content of the pods could be transformed into carbon nano- product under controlled conditions. Thermochemical conversion methods such as pyrolysis can retain and enrich carbon percentage and eject other elements. With careful selection of precursor material and processing conditions such as heating rate, residual plateau, and end temperature, it is possible to form conjugated carbons with sp^2 state with hierarchical micromesopores [24]. Porous nanocarbons can be produced in one pot process unlike templated carbons which require post processing to remove the template. The one pot process is highly acquiescent to industrial scale processing [29–34].

In the current study, the biomass of *Caesalpinia Sappan* pods was used, for the first time, to produce carbon nanoparticles. The pods were subjected to pyrolysis at different temperatures; the carbonized products obtained at corresponding temperatures were analysed using various techniques. The results allowed comprehensible insight on the particle size and more significantly, the surface features. The surface features provide an insight into understanding the role of surface area for various electrochemical applications involving only carbon- or carbon-based electrodes.

Pure carbon-based capacitors cannot meet the requirements in high energy storage. Research is now focussed enhancing the capacitance by incorporating various metal oxides, graphene composites, MXenes, ternary metal oxides [35–39], and doped carbon materials [40]. Transition metal oxides (MOx), such as RuO_2, MnO_2, which possess high theoretical pseudo-capacitance, might be a promising alternative for enhanced energy storage capacity [41]. However, most of the pseudo-capacitance comes from surface redox reactions and only the first few nanometres from the surface layer are utilized in the faradic processes. Consequently, the capacitance of MOx in bulk is much lower than the theoretical value. In addition, the poor electrical conductivity of MOx results in poor rate capability and thus limits their applications as electrode materials for high power supercapacitors. Because porous carbon nanomaterials show high surface area and good electrical conductivity, deposition of MOx onto carbon supports not only increases the effective utilization of the active materials, but also improves the electrical conductivity of the composites [42, 43].

Experimental details

Materials

The biomass was collected from Hat Yai, Songkhla province, Thailand. Tube furnace (NoPo Nanotechnologies India Pvt. Ltd.) was used to pyrolyze the raw biomass material. N_2 gas of 99.999% was used in the pyrolysis of pods. The carbonized products were analysed by various techniques; the chemical composition of products was demonstrated by energy dispersive X-ray spectroscopy (EDS, X Max 80, Oxford Instrument, United Kingdom); the morphology and particle size was determined using field emission scanning electron spectroscopy (FESEM, SEM microscope, Apreo, FEI, Czech Republic); the surface features of waste pod derived carbon nanoparticles investigated by static volumetric N_2 gas adsorption–desorption studies using BET (Brunauer–Emmett–Teller) analyzer (ASAP2460, Micromimetics, USA); X-ray diffraction (X-ray) patterns were collected using Empyrean XRD diffractometer (Empyrean, Netherland), in a 2θ range from 10° to 80° using Cu Kα radiations with a wavelength of 0.154 nm; Raman spectroscopy was performed using Raman microscope spectrometer (RAMANforce, Nanophoton, Japan); further, the thermogravimetric analysis (TGA) of raw material and the carbonized product was conducted by heating them from 50 to 1000 °C at 10.0 °C/min under N_2 atmosphere using Perkin Elmer, USA TGA 7.

Electrochemical studies on CSCNP1000 as electrode materials were done in AUTOLAB M204 potentiostat/galvanostat fitted with a frequency response analyser (FRA). The CSCNP1000 electrode material was analysed for supercapacitor behaviour by cyclic voltammetry (CV), galvanostatic charge discharge (GCD) tests, electrochemical impedance spectroscopy (EIS).

Methods

The waste pods of *Caesalpinia Sappan* (represented as CS) were used as precursor for the synthesis of carbon

nanoparticles, which were collected from Hat Yai regions of Thailand; however, the plant could be found in all parts of the world. The pods were cleaned with distilled water and dried completely in an oven. It was crushed and mixer was used to grind the pods into fine powder. The powder was collected using sieve of mesh size ~ 62 μm from vibratory shaker. The precursor powder was placed in a quartz boat and subjected to pyrolysis in a tube furnace. The followed was a catalyst free and template free, one-pot pyrolysis method in the presence of N_2 gas (flow rate: 150 cm^3/min). Pyrolysis was conducted at different temperatures, 400 °C, 600 °C, 800 °C and 1000 °C. The carbonized products were coded with simple representations as CSCNP400, CSCNP600, CSCNP800 and CSCNP1000, respectively (CSCNP: *Caesalpinia Sappan* carbon nanoparticles). The Fig. 1 illustrates the CNPs synthetic procedure step-by-step.

Results and discussion

A substantial amount of details was collected for CS pod derived carbon nanoparticles from various characterization techniques. The data were analyzed meticulously, which manifested the upgradation of morphology, size and especially surface features in parallel with the pyrolysis temperature.

Chemical composition

The chemical constitution of CSCNP materials was analysed by EDS technique; the resulted spectra are given in Fig. 2a–d. It was evident from the spectra that the products were composed of carbon in major portions. The high-intensity peak at 0.27 keV represented carbon. Further, CSCNP products also showed other low-intensity peaks, corresponding to oxygen, potassium and calcium, indicating the traces of these elements in negligible amounts.

The insets of Fig. 2 are the EDS maps, which showed the distribution of carbon in the given area; it could be noticed that with increase in pyrolysis temperature, the purple color got intensified and better distributed. Figure 2e is drawn to represent the increment in the percentage of carbon in parallel to the temperature; as a result, CSCNP1000 held the highest purity. The percentage of carbon in CSCNP400, CSCNP600, CSCNP800 and CSCNP1000 are as follows: 82, 86, 87 and 91%.

The systematic increase in the temperature drove the decomposition of biomolecules and polymeric skeleton of pod biomass, resulting in the elimination of volatile matters formed during heating process and forming the residue which was rich with carbon content. A similar observation was reported, where onion peels were pyrolyzed from 200 to 1000 °C [44]; the corresponding products showed systematic increase in carbon percentage with rise in temperature.

FTIR analysis was performed for the samples before and after pyrolysis, to demonstrate the changes occurring in

Fig. 1 Schematic representation of preparation of carbon nanoparticles from waste *Caesalpinia Sappan* pods
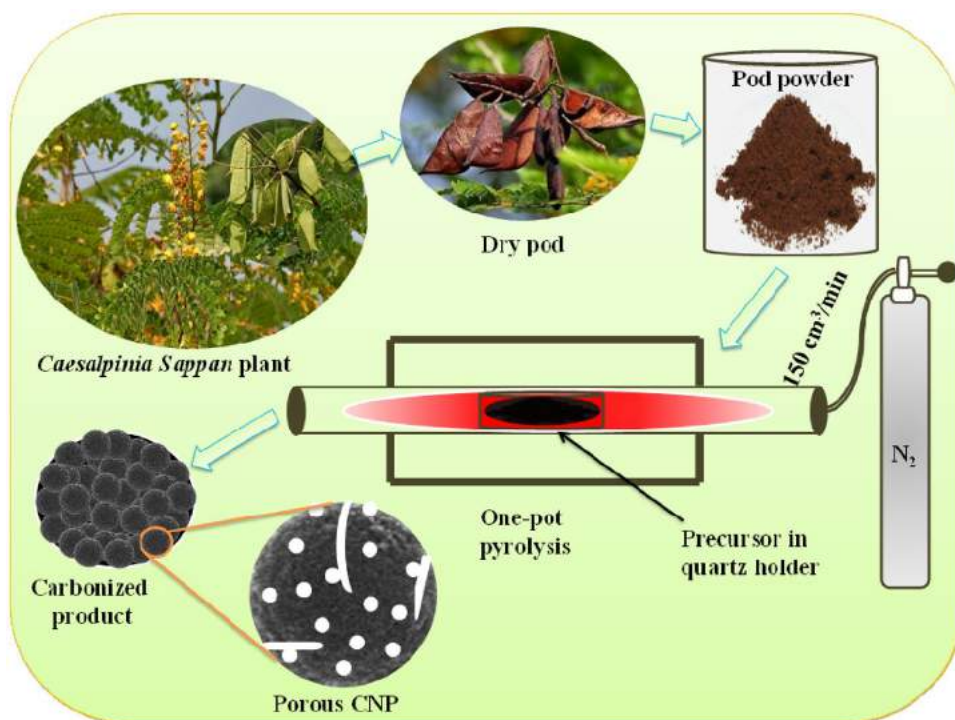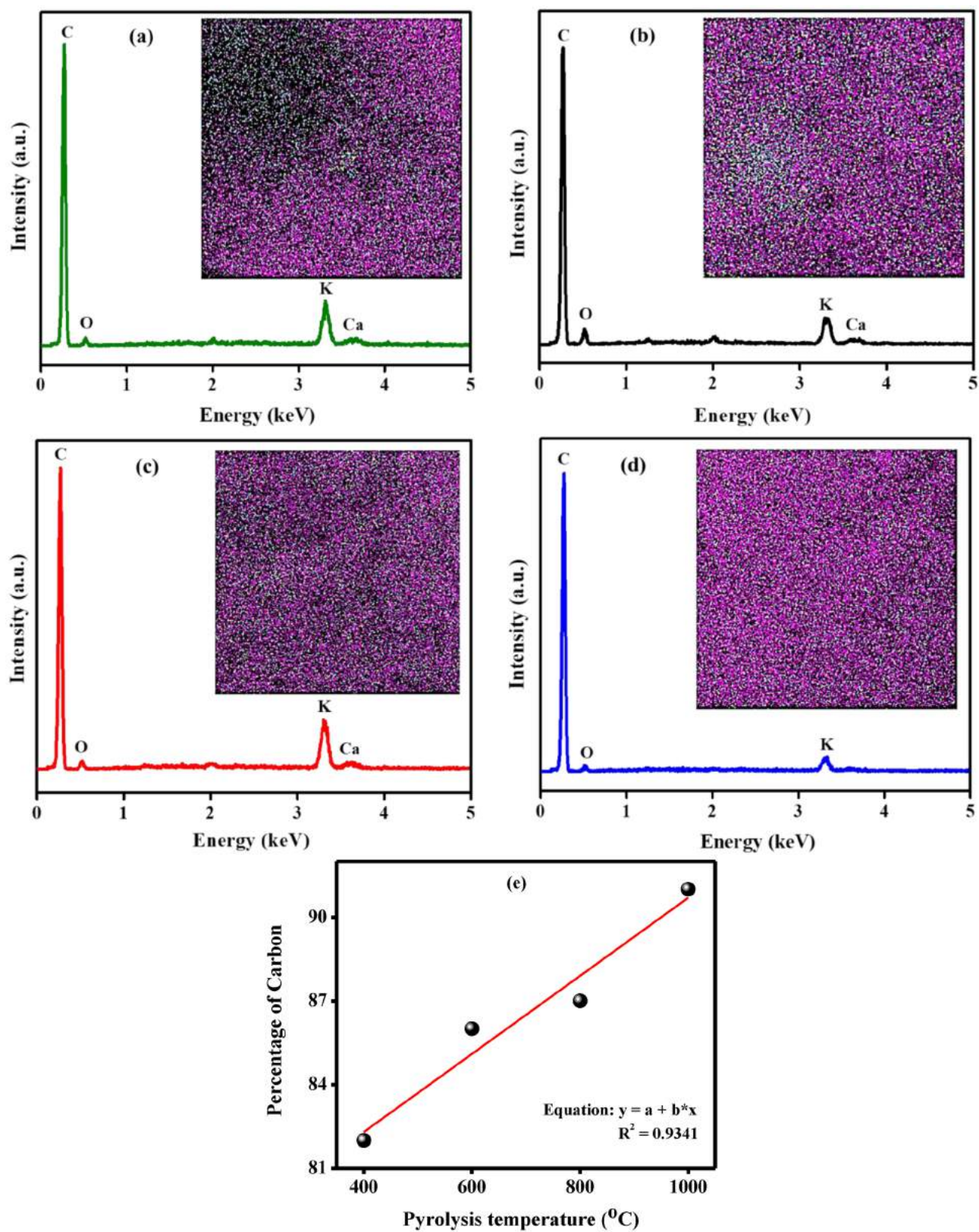
Fig. 2 **a** CSCNP400 **b** CSCNP600 **c** CSCNP800 **d** CSCNP1000 **e** plot showing increasing percentage of carbon with increase in temperature; insets are the EDS maps showing distribution of carbon nanoparticles (purple colored spots represent carbon)

the material with respect to the functional groups and their respective vibrations (Fig S1). The raw sample showed a prominent broad band at a range of 3000–3600 cm^{-1} corresponding to –O–H stretching in various biomolecules. The peak at 1573 cm^{-1} could be due to –C=C– stretching vibrations. The vibration due to –C–O– stretching appeared at 1028 cm^{-1}. After pyrolysis, a different pattern in FTIR spectrum obtained for CSCNP samples. The spectrum of CSCNP400 and the raw sample could be comparable, indicating existence of bio-molecular traces in the carbonized product. The prominent peaks disappeared in later stages, but indicating the presence of –O–H and –C–O– vibrations in minute quantities.

Morphology and grain size

The particle shape and size of CSCNP materials were analyzed using electronic microscopy. The FESEM images obtained for these materials are given in Fig. 3. It was observed that CSCNP400 material did not form any definite shape; CSCNP600 contained near to spherical shapes, whereas, the CNPs produced at higher temperatures (CSCNP800 and CSCNP1000) showed definite spherical morphology. The TEM analysis of CSCNP samples corroborated with the SEM analysis and confirmed the spherical morphology. The TEM image of CSCNP1000 is given in supplementary section for representation (Fig. S2).

Further, the carbon particles exhibited size in nanoscale range. Histograms of individual products were drawn, Fig. 4, to demonstrate the size distribution in CSCNPs. The size of nanoparticles was found to decrease when the pods were carbonized at higher temperatures. The graph (Fig. 4a) indicates reduced average particle size (110–25 nm) with respect to corresponding CSCNP materials. Reduction in particle size with increase in pyrolysis temperature occurs due to the dissociation of larger solid clusters or particles. At higher temperatures, the particles are exposed to more stress in the form of heat. In the process of releasing heat, fracture of disoriented crystallites takes place resulting in smaller particles with spherical morphology [45].

Study of surface area

The surface of CSCNP materials were studied diligently as the surface properties are the vital factors for nanoparticles that determine the material behaviour, dispersity, etc. and also makes them suitable to be applied in various significant applications such as energy storage, adsorption, catalysis, etc. Various methods were employed while analysing the surface characteristics of CNPs, to describe them cumulatively from different perspectives.

The surface area of CSCNP materials were determined by Single point, BET, Langmuir, BJH (Barrett–Joyner–Halenda), D–H (Dollimore and Heal), D–A (Dubinin–Astakhov), t-plot, MP (Mikhail et al.), DFT (Density functional theory) and NLDFT (Non-local density functional theory) methods. The Figs. 5, 6, and 7 represent the different surface area measurements obtained for CSCNP materials prepared at different temperatures from 400 to 1000 °C.

Single point method is a rapid testing method of determining accurate specific surface area of materials from

Fig. 3 FESEM images of *Caesalpinia Sappan* derived carbon nanoparticles; CSCNP400, CSCNP600, CSCNP800 and CSCNP1000
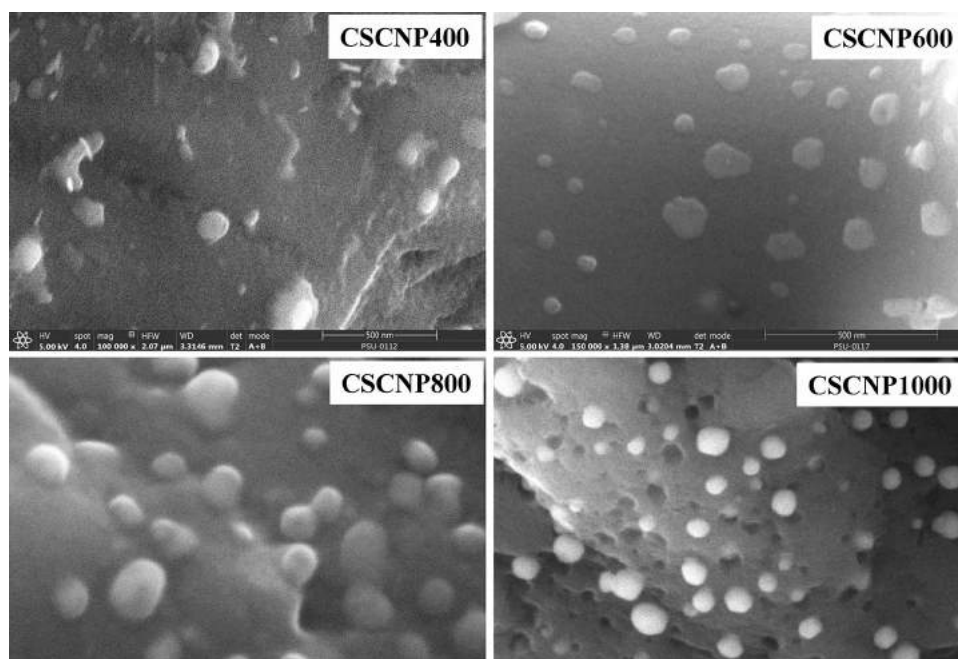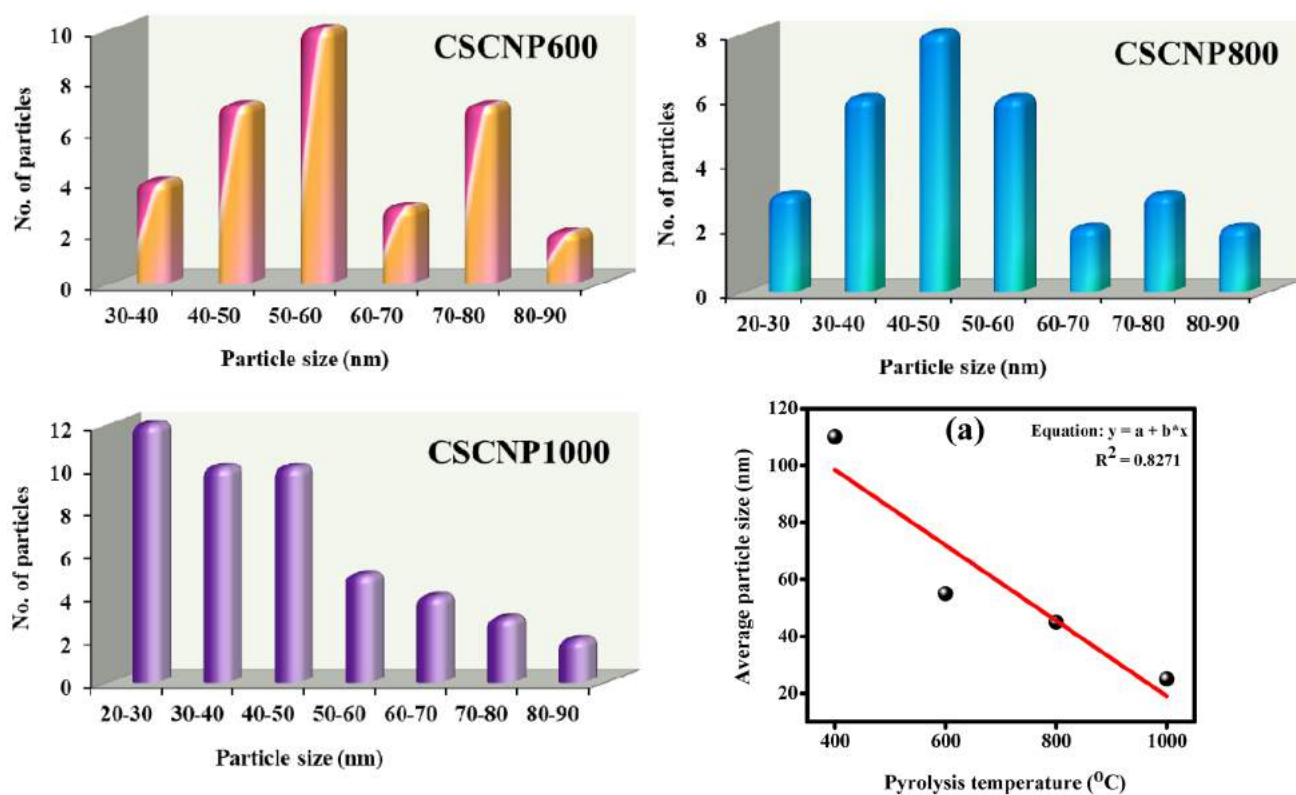
Fig. 4 Histograms showing particle size distribution of CSCNP materials; (a) represents linear fitted graph of decreasing average particle size with increase in temperature from 400 to 1000 °C
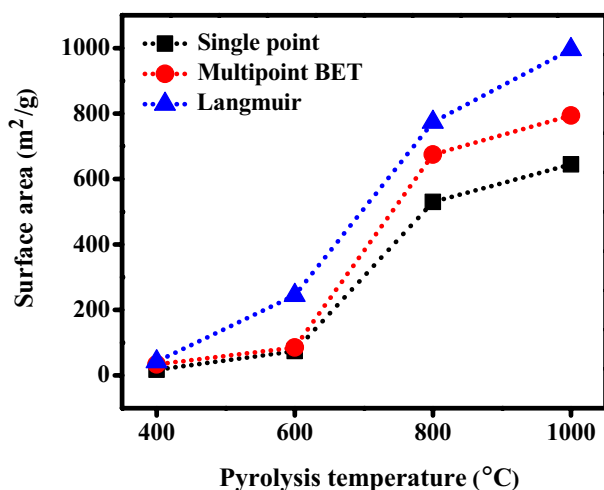
Fig. 5 The results of surface area analysis for CSCNP produced at corresponding temperatures from 400 to 1000 °C by Single point, multipoint BET and Langmiur methods

a single point on nitrogen adsorption isotherm [46]. The single point surface area values obtained for CSCNP400, CSCNP600, CSCNP800 and CSCNP1000 were 17.6, 74.4, 529.6 and 644.2 m^2/g, respectively, as shown in Fig. 5. Aside from the advantages such as simple and speed measurement,

Single point is considered to be lesser reliable than the multipoint method [47].

Multipoint BET is the commonly followed and more reliable method of determining the specific surface area, which considers the entire surface of nanomaterial, including surface of pores and external surface. Figure 5 also shows the BET surface area of corresponding CSCNP materials produced at increased temperature.

The graph confirms enhancement of active sites at surface with rise in pyrolysis temperature. The surface area values obtained for CSCNP400, CSCNP600, CSCNP800 and CSCNP1000 were 33.8, 85.7, 674.8 and 793.9 m^2/g, respectively.

The N$_2$ adsorption–desorption plots obtained for CSCNP materials are given in Fig. 6. The patterns of the curves and hysteresis loops were used to gather details about surface characteristics. The amount of gas adsorbed by CSCNP400 and CSCNP600 materials was lower than that of the CSCNP800 and CSCNP1000 products. Further, the curves appeared to follow Type II isotherm, indicating no substantial active sites and porous structures at the surface. The large hysteresis loops were H2 type, which correspond to cylindrical or spherical pores. On the other hand, the carbon particles produced at higher temperature range (CSCNP800 and CSCNP1000) showed enhanced surface features. Higher
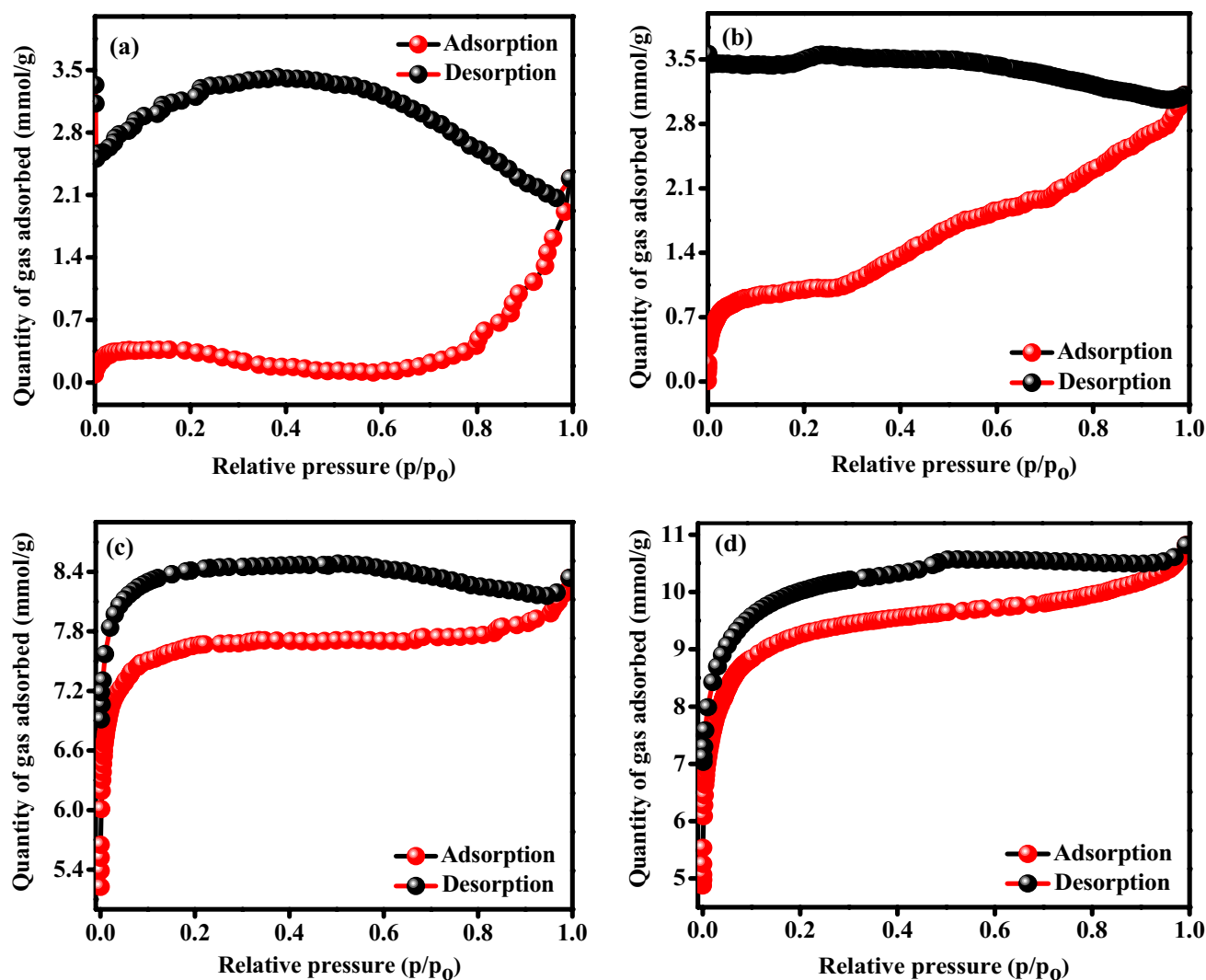
Fig. 6 N$_2$ adsorption–desorption curves of CSCNP obtained at 400 to 1000 °C; **a** CSCNP400; **b** CSCNP600; **c** CSCNP800; **d** CSCNP1000

quantity of gas was adsorbed and the curves were Type IV indicating mesoporous characteristics. Additionally, the hysteresis loop was H4 type which suggested the existence of micropores [48]. Therefore, it could be inferred that CSCNP800 and CSCNP1000 were microporous/mesoporous solids. The porous structures were attributed to cause large surface area in these materials.

The surface area of CSCNP materials was also determined by Langmuir method. The corresponding surface area values obtained are drawn in Fig. 5 (42.1, 244.8, 773.9 and 995.6 m^2/g for CSCNP400, CSCNP600, CSCNP800 and CSCNP1000, respectively). But the Langmuir method is considered to be more applicable to chemisorption than physical adsorption [49]; but could be applied to physisorption isotherms of Type I (as in microporous solids). This is because the method is limited strictly to one molecular layer [50], which cannot be exceeded. But the physical adsorption

of N$_2$ gas does not always cease to monolayer formation (as in CSCNP materials which exhibited Type II and Type IV isotherms) [51]. Also, CSCNP materials have shown to possess micropores and mesopores; in this regard, Langmuir method could be considered as less effective to determine the surface area.

Surface area in pores is evaluated by various methods, as shown in Fig. 7. The BJH, DFT/NLDFT, t-plot, D-A and MP methods showed a common trend similar to Single point, BET and Langmuir methods of determining surface area values. The surface area determined by each method is given in Table 1. With rise in carbonization temperature, there observed significant increase in the surface features of CSCNP materials. While the difference in surface area between CSCNP400 and CSCNP600 was less, a sharp increase was observed from CSCNP600 to CSCNP800 and CSCCNP1000. This could be attributed to the well-defined
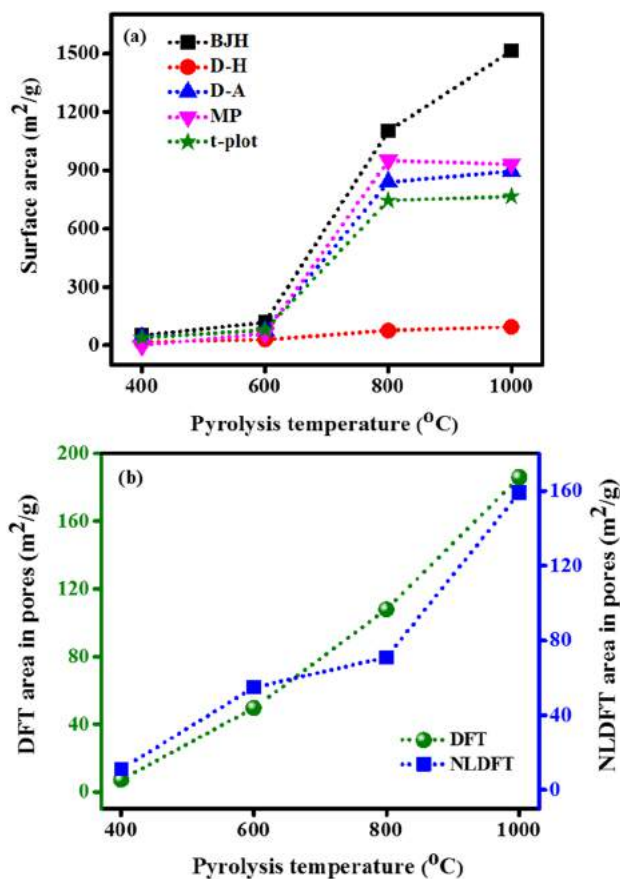
Fig. 7 Surface area in pores determined by **a** BJH, D-H, D-A, MP and t-plot methods; and **b** DFT and NLDFT methods

porous spherical nanostructures formed at ≥ 800 °C, as perceived from FESEM images.

t-plots were obtained for CSCNP materials are given in the Fig. 8, as representation of microporous structures. The plots of CSCNP400 and CSCNP600 showed straight line, indicating the absence of significant porosity; further, the pattern obtained for CSCNP800 and CSCNP1000 was Type I which corresponded to microporous materials [52]. The filling of narrow micropores took place at lower vapour pressures [53], above which the interaction between adsorbate-adsorbent resulted in secondary filling in larger micropores at a vapour pressure up to 0.01–0.2 [54]. Moreover, the t-plot surface area of CSCNP materials was found to increase with increase in pyrolysis temperature.

Pore analysis

The evaluation of pores was conducted by different methods. The average pore width obtained for CSCNP materials from BET, BJH, D–H, H–K (Horvath and Kawazoe) and MP methods are given in Table 2; the same is illustrated in the Fig. 9. It could be demonstrated from the graphs that

Table 1 Surface area of CSCNP materials determined by different methods

Material	Single point (m²/g)	BET (m²/g)	Langmuir (m²/g)	BJH (m²/g)	D–H (m²/g)	DFT (m²/g)	NLDFT (m²/g)	t-plot (m²/g)	D–A (m²/g)	MP (m²/g)
CSCNP400	17.6	33.8	42.1	50.4	17.2	7.1	11.2	40.0	42.6	0
CSCNP600	74.4	85.7	244.8	119.3	76.7	49.6	54.9	79.8	78.3	62.1
CSCNP800	529.6	674.8	773.9	1102.7	30.4	107.8	70.9	745.8	841.0	950.6
CSCNP1000	644.2	793.9	995.6	1515.2	95.7	185.9	159.1	766.9	894.5	932.1
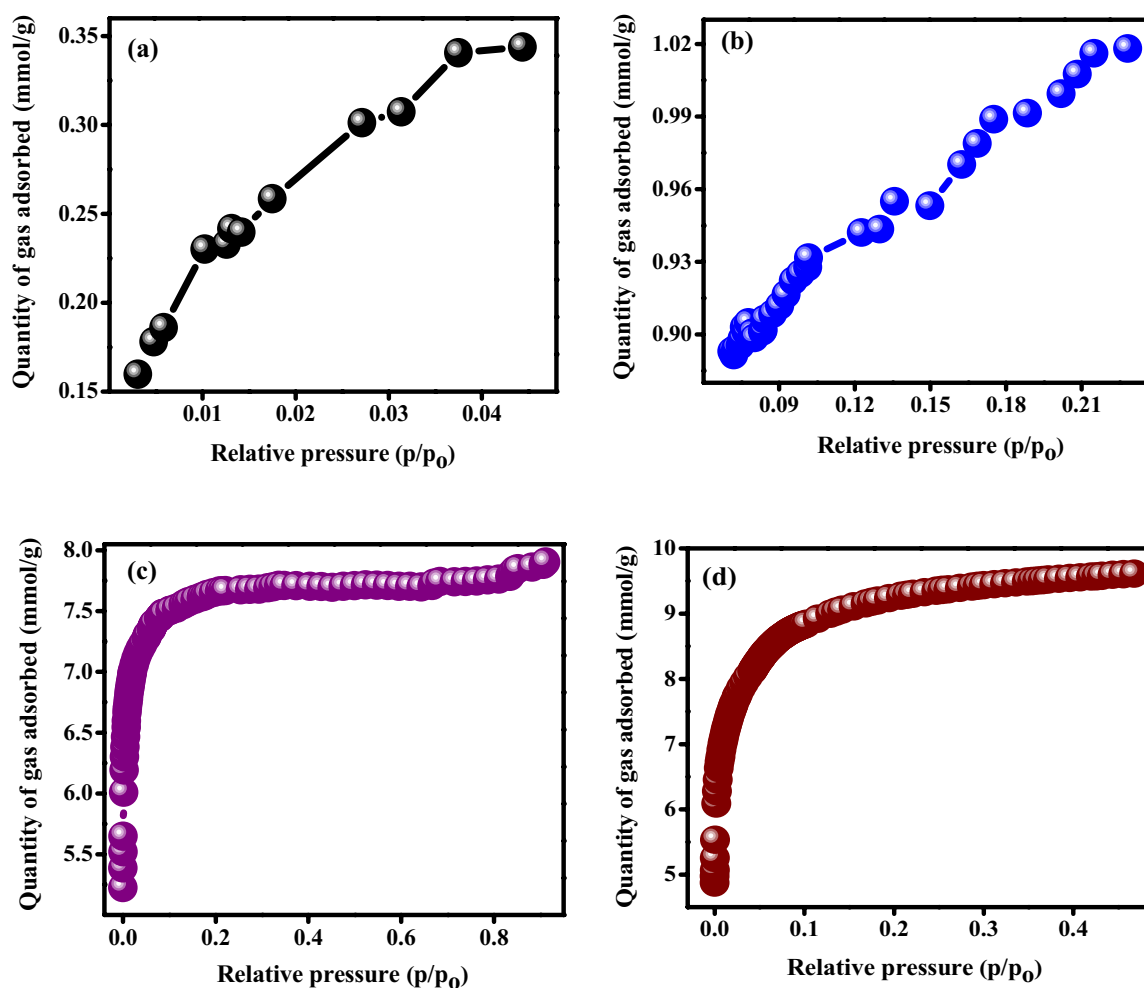
Fig. 8 t-plots obtained for **a** CSCNP400; **b** CSCNP600; **c** CSCNP800; and **d** CSCNP1000

Table 2 Pore width of CSCNP materials determined by different methods

Material	BET (nm)	BJH (nm)	D–H (nm)	H–K (nm)	MP (nm)
CSCNP400	8.5	6.1	20.2	0.7	0.0
CSCNP600	5	3.2	5.5	0.7	0.9
CSCNP800	1.9	1	5.1	0.5	0.3
CSCNP1000	1.7	1.1	3.9	0.5	0.4

the products were mesoporous/microporous in nature, as the average pore width is ≤ 20.2 nm. Furthermore, the pore size was found to reduce in the materials produced at higher pyrolysis temperatures and this was the common trend in all the methods. Beyond 600 °C, no significant difference in the pore size was observed, and the size also lied near to microporous region, possibly making them suitable materials for the fabrication of energy storage devices [55].

Pore volumes obtained for CSCNP materials from 400 to 1000 °C are given in Table 3; Figure 10 represents pore volume corresponding to the CSCNP materials. It was evident from the results that the carbon nanoparticles produced

at 800 and 1000 °C (CSCNP800 and CSCNP1000, respectively) were highly porous in nature, whereas CSCNP400 and CSCNP600 did not show significant values. The D–H, H–K and MP methods signified the micropores; also, D–H method was useful to give an estimation of the cylindrical pores [56]; H–K method was considered to be effective for highly microporous carbon materials [57].

Further, MP method is the extension of t-plot method which analyses micropores of slit shape [58, 59]. Thus the study of CSCNP surface by different methods helped to demonstrate the overall surface properties of the materials, such as surface area, pore size and shapes.
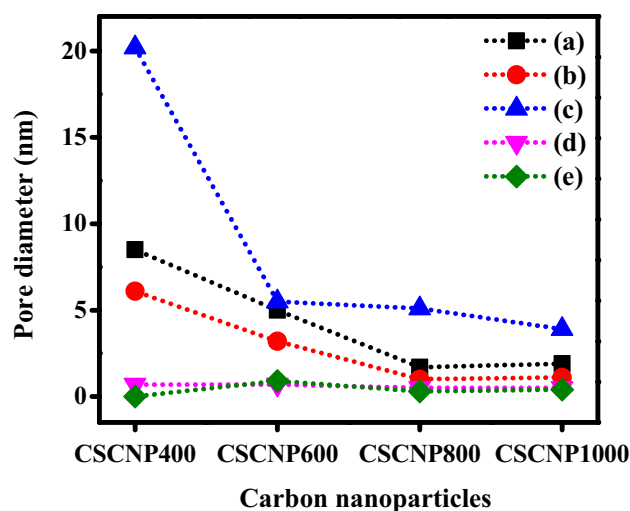
Fig. 9 Graph illustrating pore width in CSCNP materials from CSCNP400 to CSCNP1000

Fig. 10 Illustration of pore volume corresponding to the CSCNP materials obtained from 400 to 1000 °C

Pore size distribution curves were drawn for the CSCNP materials using the BJH data in Fig. 11. The graphs clearly showed the volume of variable sized pores; the pore volumes were larger towards microporous region (< 2 nm). The CSCNP400 and CSCNP600 materials indicated pores in a wide size range, whereas the CSCNP800 and CSCNP1000 materials indicated well-defined porous structure constituted by mesopores and the large volume of micropores.

Influence of temperature on surface features

The analysis of surface parameters provided facts about the influence of pyrolysis temperature on the porous surface of CSCNP materials. In the study, temperature has been utilized as a tool to surface engineer the carbon nanomaterials. It is evident from the earlier explanations that the surface area and pore volume raise with progressive increase in the pyrolysis temperature from 400 to 1000 °C. The increase in these properties could be attributed to the decomposition of cellulosic matters (> 600 °C) and the subsequent removal of volatile matters, creating rudimentary pores in the material. Further, when the biomass was exposed to larger heat (at a

rate of 10 °C/min) as in CSCNP800 and CSCNP1000, temperature reached quickly into the material, resulting in the enhancement of cellulose decomposition and volatile matter extraction. While nitrogen gets diffused easily into the core of the material in this condition, it forms large volume of pores and surface area.

The morphological and surface studies confirmed that the CSCNP1000, produced at 1000 °C, exhibited the enhanced features compared to the other CSCNP materials, with respect to well defined spherical shape, small grain size and excellent surface area and porous nature. Therefore, the CSCNP1000 sample was considered for further material analysis to understand the physical and chemical aspects.

Thermal stability of CSCNP by TGA

The thermal stability of CSCNP1000 was studied by TGA analysis. A known weight of raw biomass and CSCNP1000 was heated from room temperature to 1000 °C and the weight loss with respect to temperature was drawn in Fig. 12. The TGA graph of raw material (Fig. 12a) showed large loss in weight because of decomposition of biomolecules during the heating process; reduction of weight up to ~ 120 °C was

Table 3 Pore volume of CSCNP materials determined by different methods

Material	Single point (cm³/g)	BJH (cm³/g)	DFT (cm³/g)	NLDFT (cm³/g)	t-plot (cm³/g)	H–K (cm³/g)	D–A (cm³/g)	MP (cm³/g)
CSCNP400	0.07	0	0.08	0.08	0.07	0.01	0.02	0
CSCNP600	0.11	0.02	0.1	0.1	0.1	0.03	0.04	0.05
CSCNP800	0.29	0.04	0.27	0.24	0.26	0.26	0.3	0.27
CSCNP1000	0.37	0.05	0.43	0.32	0.36	0.32	0.37	0.36
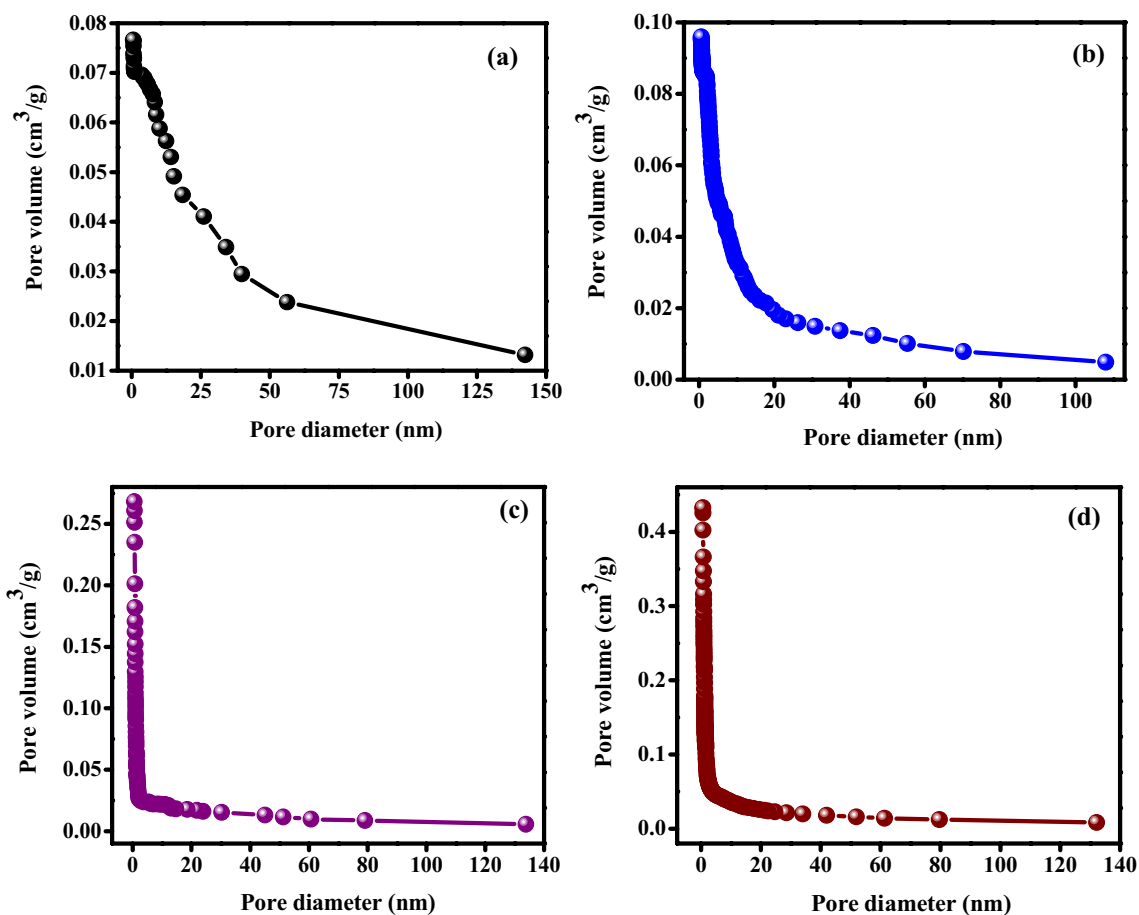
Fig. 11 Pore size distribution curves obtained for **a** CSCNP400, **b** CSCNP600, **c** CSCNP800 and **d** CSCNP1000
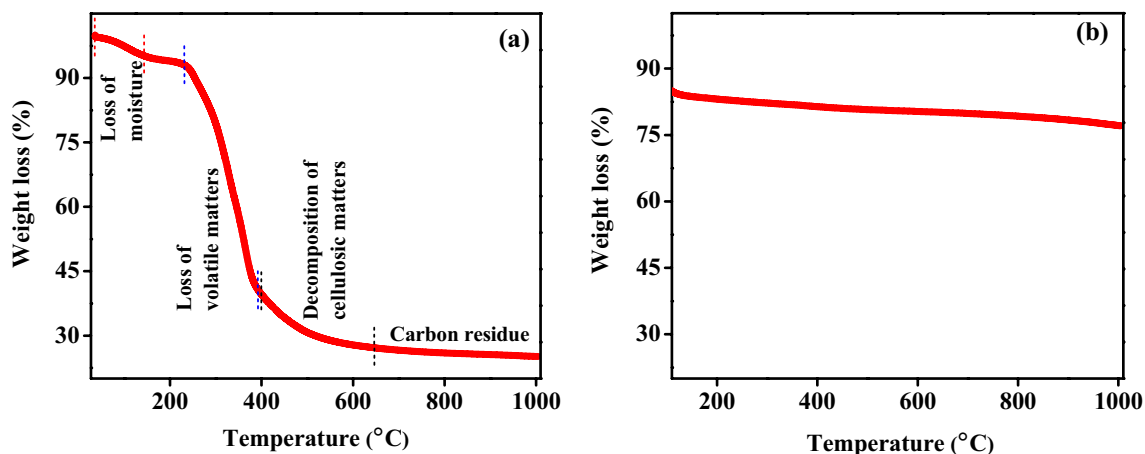
Fig. 12 TGA plots showing loss of weight with respect to temperature; **a** Raw CS material; **b** CSCNP1000

due to removal of water content. Elimination of volatile matters occurred up to ~230 °C; beyond this temperature, a huge dip in the weight was caused up to 640 °C, which could be attributed to the decomposition of biopolymers (cellulosic components) [60].

The disintegration of lignocellulosic component occurred at higher temperatures beyond 600 °C; no significant weight loss was observed at ≥ 800 °C indicating the formation of stable carbon residue, which also

corroborated with the high purity and excellent features of CSCNP materials produced in this temperature range.

On the other hand, the TGA plot of CSCNP1000 (Fig. 12b) showed no remarkable reduction in weight up to 1000 °C, confirming the outstanding thermal stability of the material. Therefore, this porous material could be utilized in the applications which require harsh temperature conditions.

Physico-chemical analysis of CSCNP by XRD and Raman spectroscopy

The CSCNP1000 was subjected to XRD and Raman spectroscopic analysis to demonstrate the physical and chemical structure of CSCNP1000 material. The XRD spectrum obtained for CSCNP1000 is given in Fig. 13a. The pattern showed two prominent peaks at $2\theta = 24°$ and $44°$, corresponding to carbon. The broad bands indicated that the carbon product was amorphous in nature. Further, a peak was observed at $26°$ which could be attributed to the graphitic nature present in the carbon matrix. A peak formed at $31°$ could be due to the traces of calcium oxides or carbonates. The XRD analysis of other CSCNP samples also demonstrated structural arrangement of carbon atoms in these materials (Fig S3). The XRD patterns showed two predominate broad bands at a range of $2\theta = 20°$ and $30°$ (002) and at $\sim 45°$ (100). The broad bands indicated amorphous nature of CNPs. The other small sharp peaks could be due to trace elements such as calcium and potassium.

Raman spectroscopy was performed to demonstrate the order in the carbon structure. The graph obtained (Fig. 13b) showed two sharp peaks at 1344 and 1595 cm^{-1}, called D band and G band, respectively. D band, generally, represents disorder in the structure and G band corresponds to graphitic nature. In CSCNP1000, the intensity of D band was higher than the G band; this could be attributed to the bending of graphic layers at the curvatures of spherical shaped carbon nanoparticles. Small size of the particles, as discussed under SEM analysis, led to the larger bending of carbon layers, which resulted in the prominent D band intensity [44, 59]. However, the rise of G band confirmed graphitic carbons; further, an additional graphitic band was observed at a range of 2500–3000 cm^{-1}. The Raman spectroscopic analysis was also carried out for other CSCNP samples too. The spectra showed two prominent peaks at 1340 cm^{-1} and 1598 cm^{-1}, (Fig. S4) where the former represented imperfections in the material lattice and the latter indicated the graphitic order of the carbon atoms. It could be observed that the D band intensity progressively increased with increase in pyrolysis temperature. This could be attributed to the decrease in particle size. As particle size decreases, more and more bending of the carbon layers takes place at the curvature of spheres, resulting in higher strain and more number of dangling bonds at the curved surface.

Electrochemical performance of CSCNP1000

For evaluation of electrochemical performance of CSCNP1000, electrode was prepared using the homogeneous mixture of CSCNP1000, polyvinylidene difluoride (PVDF) and carbon black in 9:1:1 ratio using N-methyl pyrrolidone (NMP) as the solvent. This mixture was coated on nickel foam current collector (1×1 cm^2 area). A more detailed procedure for the electrode preparation is reported in our earlier works [61–64].

The cyclic voltammetry (CV) was carried out at the potential window of -1.0–0 V in a three-electrode setup using CSCNP1000 coated Ni foam as working electrode and 1.0 M KOH as electrolyte, the other two electrodes being
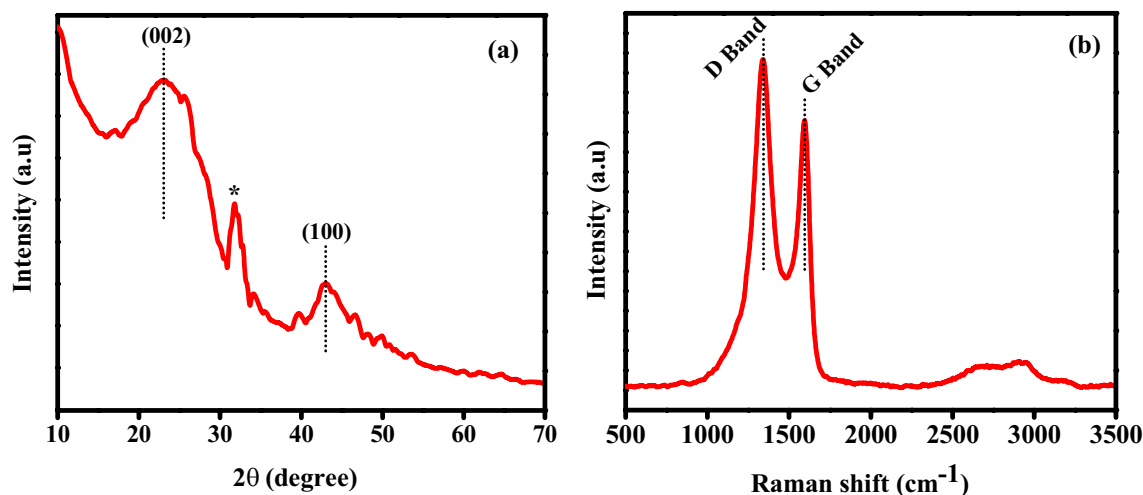
Fig. 13 **a** XRD and **b** Raman spectroscopic plots obtained for CSCNP1000
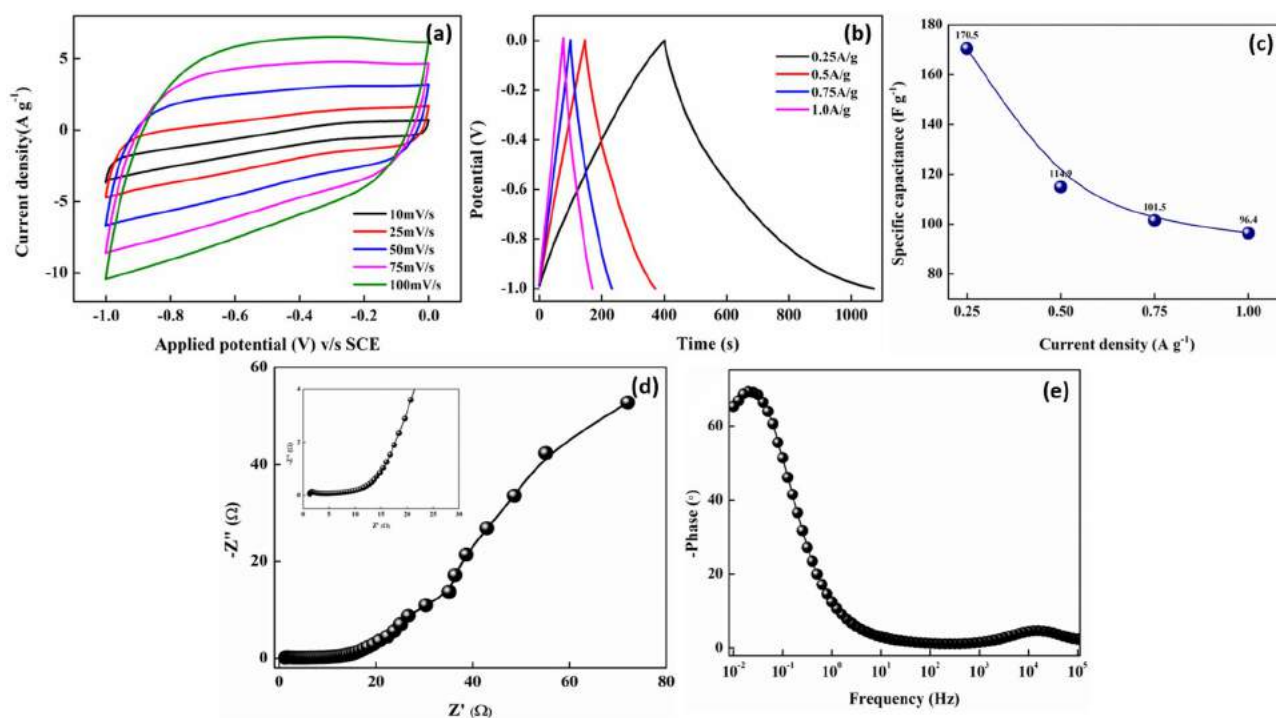
Fig. 14 Cyclic voltammetry plot (**a**) and galvanostatic charge discharge curves (**b**) of CSCNP1000 electrode at different scan rates and different current densities, respectively, plot of specific capacitance as function of current density (**c**), Nyquist impedance plot (**d**), inset shows the high-frequency region, Bode plot (**e**) as function of frequency of CSCNP1000 electrode in 1.0 M KOH electrolyte

saturated calomel electrode (SCE) and platinum rod as reference and counter electrode, respectively. The CV plot at different scan rates (Fig. 14a) ranging from 10 to 100 mV s^{-1} shows rectangular shape without redox peaks, which is typical of materials exhibiting EDLC behaviour. The non-Faradaic charge transfer was further confirmed from galvanostatic charge discharge (GCD) tests carried out at potential window of − 1.0–0 V (Fig. 14b) at current densities. The plot shows symmetric triangular shape with longer discharge times at lower current densities. Specific capacitance was calculated from formula reported in earlier work [64]. Maximum specific capacitance of 170.5 F/g was obtained at 0.25 A/g. Figure 14c shows the variation of specific capacitance as function of current density. Impedance of the system was analysed from 100 kHz to 0.01 Hz, at 10 mV with AC current amplitude signal at open circuit potential. The Nyquist impedance plot (Fig. 14d) shows a semi-circular curve followed by a 45° vertical tail. The R_S and R_{CT} values of 1.3 Ω and 0.6 Ω were obtained after fitting the impedance data with the equivalent circuit. Variation of phase angle with frequency was plotted in Fig. 14e. The low impedance values and high capacitance indicate that CSCNP1000 can be used as electrode material in supercapacitors. The electrochemical results were compared with some of the earlier reports. Table S3 compares the surface area of the carbon material and the specific capacitance obtained. In some cases

when the surface area was high (∼ 2900 m^2/g) the capacitance observed was less (189 F/g) [55], And in some other cases, surface area was moderately high (∼ 1000 m^2/g) while capacitance was high (∼ 330 F/g) [65]. There are also reports where carbon materials with lower surface area (440.7 m^2/g) have shown a high capacitance (356 F/g) [63]. Hence it can be concluded that, though there exists a direct relationship between surface area and capacitance, the extent of surface actually available for the ions and electrode kinetics play role in increased or decreased capacitance. Detailed investigation on various parameters related to energy storage device study in progress and will be reported elsewhere.

Conclusions

Surface engineered carbon nanoparticles were prepared by pyrolysing the waste seed covers of *Caesalpinia Sappan* plant at different temperatures from 400 to 1000 °C, in a single step. The carbonized products were rich in carbon content and the material produced 1000 °C, CSCNP1000 exhibited the excellent purity (91% of carbon) and well-defined spherical shape with small grain size (∼ 30 nm). A detailed investigation of surface features of CSCNP400 to CSCNP1000 samples was carried out using various methods such as Single point/multipoint BET, BJH, Langmuir, D–H,

D–A, t-plot, H–K, DFT/NLDFT and MP methods. All these methods showed a similar trend of improved surface area and pore volume for carbon nanoparticles produced at higher temperatures (≥ 800 °C). The CSCNP1000 exhibited the highest surface area of 794 m²/g and 1515 m²/g, determined by BET and BJH methods, respectively. The maximum pore volume obtained for CSCNP1000 was 0.37 cm³/g. The surface analysis by various methods helped to demonstrate the surface features from different aspects, such as adsorption by pores of variable size and shape. Further, the analyses confirmed that the porous structure of carbon samples was constituted by micropores and mesopores. Therefore, the charge holding capacity of CSCNP1000 was tested by performing electrochemical experiments, which determined the specific capacitance of 170.5 F/g at 0.25 A/g. It confirmed the suitability of these porous materials for the fabrication of cost effective energy storage devices (supercapacitors).

References

1. Gatoo, M.A., Naseem, S., Arfat, M.Y., Mahmood Dar, A., Qasim, K., Zubair, S.: Physicochemical properties of nanomaterials: Implication in associated toxic manifestations. BioMed. Res. Int. **2014**, 1–8 (2014)

2. Lehn, J.-M.: Toward self-organization and complex matter. Science **295**(5564), 2400–2403 (2002)

3. Li, K., Ma, C.F., Ling, Y., Li, M., Gao, Q., Luo, W.J.J.M.C.: Physics, Acid/base bifunctional carbonaceous nanomaterial with large surface area: Preparation, characterization, and adsorption properties for cationic and anionic compounds. Mater. Chem. Phys. **162**, 149–161 (2015)

4. Mane, G.P., Talapaneni, S.N., Anand, C., Varghese, S., Iwai, H., Ji, Q., Ariga, K., Mori, T., Vinu, A.: Preparation of highly ordered nitrogen-containing mesoporous carbon from a gelatin biomolecule and its excellent sensing of acetic acid. Adv. Funct. Mater. **22**(17), 3596–3604 (2012)

5. Raymundo-Piñero, E., Cadek, M., Béguin, F.: Tuning carbon materials for supercapacitors by direct pyrolysis of seaweeds. Adv. Funct. Mater. **19**(7), 1032–1039 (2009)

6. Zhu, Z., Jiang, H., Guo, S., Cheng, Q., Hu, Y., Li, C.J.S.R.: Dual tuning of biomass-derived hierarchical carbon nanostructures for supercapacitors: the role of balanced meso/microporosity and grapheme. Sci. Rep. **5**, 15936 (2015)

7. Lee, J., Kim, J., Hyeon, T.: Recent progress in the synthesis of porous carbon materials. Adv. Mater. **18**(16), 2073–2094 (2006)

8. Hulicova-Jurcakova, D., Seredych, M., Lu, G.Q., Bandosz, T.J.: Combined effect of nitrogen- and oxygen-containing functional groups of microporous activated carbon on its electrochemical performance in supercapacitors. Adv. Funct. Mater. **19**(3), 438–447 (2009)

9. Xu, B., Chen, Y., Wei, G., Cao, G., Zhang, H., Yang, Y.: Activated carbon with high capacitance prepared by NaOH activation for supercapacitors. Mater. Chem. Phys. **124**(1), 504–509 (2010)

10. Rose, M., Korenblit, Y., Kockrick, E., Borchardt, L., Oschatz, M., Kaskel, S., Yushin, G.: Hierarchical micro- and mesoporous carbide-derived carbon as a high-performance electrode material in supercapacitors. Small **7**(8), 1108–1117 (2011)

11. Taer, E., Deraman, M., Talib, I., Awitdrus, A., Hashmi, S., Umar, A.: Preparation of a highly porous binderless activated carbon monolith from rubber wood sawdust by a multi-step activation process for application in supercapacitors. Int. J. Electrochem. Sci **6**(8), 3301–3315 (2011)

12. Borchardt, L., Zhu, Q.-L., Casco, M.E., Berger, R., Zhuang, X., Kaskel, S., Feng, X., Xu, Q.J.M.T.: Toward a molecular design of porous carbon materials. Mater. Today **20**(10), 592–610 (2017)

13. Yang, H., Ye, S., Zhou, J., Liang, T.: Biomass-derived porous carbon materials for supercapacitor. Front. Chem. **7**, 1–17 (2019)

14. Liu, C., Yan, X., Hu, F., Gao, G., Wu, G., Yang, X.: Toward superior capacitive energy storage: recent advances in pore engineering for dense electrodes. J. Adv. Mater. **30**(17), 1705713(1–14) (2018)

15. Supriya, S., Shetti, V.S., Hegde, G.: Conjugated systems of porphyrin–carbon nanoallotropes: a review. New J. Chem. **42**(15), 12328–12348 (2018)

16. Satapathy, P., Adiga, R., Kumar, M., Hegde, G., Prasad, S.K.: Porous nanocarbon particles drive large magnitude and fast photomechanical actuators. J. Nanostruct. Chem. (2021). https://doi.org/10.1007/s40097-021-00414-9

17. Rastogi, A., Pandey, F.P., Parmar, A.S., Singh, S., Hegde, G., Manohar, R.: Effect of carbonaceous oil palm leaf quantum dot dispersion in nematic liquid crystal on zeta potential, optical texture and dielectric properties. J. Nanostruct. Chem. (2021). https://doi.org/10.1007/s40097-020-00382-6

18. Kanagavalli, P., Pandey, G.R., Bhat, V.S., Veerapandian, M., Hegde, G.: Nitrogenatedcarbon nanoelectrocatalyst advertently processed from bio-waste of Allium sativum for oxygen reduction reaction. J. Nanostruct. Chem. (2021). https://doi.org/10.1007/s40097-020-00370-w

19. John, A., Benny, L., Cherian, A.R., Narahari, S.Y., Varghese, A., Hegde, G.: Electrochemical sensors using conducting polymer/noble metal nanoparticle nanocomposites for the detection of various analytes: a review. J. Nanostruct. Chem. **11**, 1–31 (2021). https://doi.org/10.1007/s40097-020-00372-8

20. Ji, Y., Wang, S., Dong, Y., Li, L., Li, L., Feng, X., Lu, X., Mu, L.: Tuning nitrogen species on natural biomass derived porous carbon for efficient acetone adsorption. Mater. Chem. Phys. **253**, 123338 (2020)

21. Liu, Y., Chen, J., Cui, B., Yin, P., Zhang, C.: Design and preparation of biomass-derived carbon materials for supercapacitors: a review. C **4**(4), 1–32 (2018)

22. De, S., Balu, A.M., van der Waal, J.C., Luque, R.: Biomass-derived porous carbon materials: synthesis and catalytic applications. J. ChemCatChem **7**(11), 1608–1629 (2015)

23. Wang, L., Hu, X.: Recent advances in porous carbon materials for electrochemical energy storage. Chem. Asian J. **13**(12), 1518–1529 (2018)

24. Deng, J., Li, M., Wang, Y.: Biomass-derived carbon: synthesis and applications in energy storage and conversion. Green Chem. **18**(18), 4824–4854 (2016)

25. Upare, D.P., Yoon, S., Lee, C.W.: Nano-structured porous carbon materials for catalysis and energy storage. Korean J. Chem. Eng. **28**(3), 731–743 (2011)

26. Ghosh, S., Santhosh, R., Jeniffer, S., Raghavan, V., Jacob, G., Nanaji, K., Kollu, P., Jeong, S.K., Grace, A.N.: Natural biomass derived hard carbon and activated carbons as electrochemical supercapacitor electrodes. Sci. Rep. **9**(1), 16315 (2019)

27. Zhou, X., Li, H., Yang, J.: Biomass-derived activated carbon materials with plentiful heteroatoms for high-performance electrochemical capacitor electrodes. J. Energy Chem. **25**(1), 35–40 (2016)

28. Senthilkumar, N., Murugesan, S., Banu, N., Supriya, S., Rajeshkannan, C.: Biochemical estimation and antimicrobial activities of the extracts of Caesalpinia Sappan Linn. J Bangladesh J. Sci. Ind. Res. **46**(4), 429–436 (2011)

29. Sakintuna, B., Yürüm, Y.: Templated porous carbons: A review article. Ind. Eng. Chem. Res. **44**(9), 2893–2902 (2005)

30. Wan, Y., Shi, Y., Zhao, D.: Supramolecular aggregates as templates: Ordered mesoporous polymers and carbons. Chem. Mater. **20**(3), 932–945 (2008)

31. Zhao, J., Niu, W., Zhang, L., Cai, H., Han, M., Yuan, Y., Majeed, S., Anjum, S., Xu, G.: A template-free and surfactant-free method for high-yield synthesis of highly monodisperse 3-aminophenol–formaldehyde resin and carbon nano/microspheres. Macromolecules **46**(1), 140–145 (2013)

32. Chen, D., Zhou, H., Li, H., Chen, J., Li, S., Zheng, F.: Self-template synthesis of biomass-derived 3D hierarchical N-doped porous carbon for simultaneous determination of dihydroxybenzene isomers. Sci. Rep. **7**(1), 1–10 (2017)

33. Yang, W., Hou, L., Xu, X., Li, Z., Ma, X., Yang, F., Li, Y.: Carbon nitride template-directed fabrication of nitrogen-rich porous graphene-like carbon for high performance supercapacitors. Carbon **130**, 325–332 (2018)

34. Xu, Z., Chen, J., Zhang, X., Song, Q., Wu, J., Ding, L., Zhang, C., Zhu, H., Cui, H.: Template-free preparation of nitrogen-doped activated carbon with porous architecture for high-performance supercapacitors. Microporous Mesoporous Mater. **276**, 280–291 (2019)

35. Krishnan, S.G., Arulraj, A., Khalid, M., Reddy, M.V., Jose, R.: Energy storage in metal cobaltite electrodes: Opportunities & challenges in magnesium cobalt oxide. Renew. Sustain. Energy Rev. **141**, 110798 (2021)

36. Dall'Agnese, Y., Rozier, P., Taberna, P.-L., Gogotsi, Y., Simon, P.: Capacitance of two-dimensional titanium carbide (MXene) and MXene/carbon nanotube composites in organic electrolytes. J. Power Sources **306**, 510–515 (2016)

37. Mukherjee, S., Ren, Z., Singh, G.: Beyond graphene anode materials for emerging metal ion batteries and supercapacitors. Nano-Micro Lett. **10**(4), 1–27 (2018)

38. Hu, M., Zhang, H., Hu, T., Fan, B., Wang, X., Li, Z.: Emerging 2D MXenes for supercapacitors: status, challenges and prospects. Chem. Soc. Rev. **49**(18), 6666–6693 (2020)

39. Sun, B., Zhang, Q., Zhang, C., Xu, W., Wang, J., Yuan, G., Lv, W., Li, X., Yang, N.: A passionfruit-like carbon-confined Cu2ZnSnS4 anode for ultralong-life sodium storage. Adv. Energy Mater. **11**(17), 2100082 (2021)

40. Wang, Z., Tan, Y., Yang, Y., Zhao, X., Liu, Y., Niu, L., Tichnell, B., Kong, L., Kang, L., Liu, Z., Ran, F.: Pomelo peels-derived porous activated carbon microsheets dual-doped with nitrogen and phosphorus for high performance electrochemical capacitors. J. Power Sources **378**, 499–510 (2018)

41. An, C., Zhang, Y., Guo, H., Wang, Y.: Metal oxide-based supercapacitors: progress and prospectives. Nanoscale Adv. **1**(12), 4644–4658 (2019)

42. Ma, H., Chen, Z., Gao, X., Liu, W., Zhu, H.: 3D hierarchically gold-nanoparticle-decorated porous carbon for high-performance supercapacitors. Sci. Rep. **9**(1), 17065 (2019)

43. Zhai, Y., Dou, Y., Zhao, D., Fulvio, P.F., Mayes, R.T., Dai, S.: Carbon materials for chemical capacitive energy storage. Adv. Mater. **23**(42), 4828–4850 (2011)

44. Supriya, S., Sriram, G., Ngaini, Z., Kavitha, C., Kurkuri, M., De Padova, I.P., Hegde, G.: The role of temperature on physical–chemical properties of green synthesized porous carbon nanoparticles. Waste Biomass Valoriz. **11**, 3821–3831 (2020)

45. Fu, G., Li, Q., Ye, J., Han, J., Wang, J., Zhai, L., Zhu, Y.: Hierarchical porous carbon with high nitrogen content derived from plant waste (pomelo peel) for supercapacitor. J. Mater. Sci. Mater.: Electron. **29**(9), 7707–7717 (2018)

46. Dollimore, D., Spooner, P.: A single point method for evaluating the specific surface area of a solid from nitrogen adsorption isotherms. J. Appl. Chem. Biotechnol. **24**(1–2), 35–41 (1974)

47. Lowell, S., Shields, J.E.: The single point BET method [13], Powder Surface Area and Porosity, pp. 30–34. Springer (1991)

48. Thommes, M., Kaneko, K., Neimark, A.V., Olivier, J.P., Rodriguez-Reinoso, F., Rouquerol, J., Sing, K.S.W.: Physisorption of gases, with special reference to the evaluation of surface area and pore size distribution (IUPAC Technical Report). Pure Appl. Chem. **87**(9–10), 1051–1069 (2015)

49. Lowell, S., Shields, J.E., Thomas, M.A., Thommes, M.: Surface area analysis from the langmuir and bet theories, Characterization of Porous Solids and Powders: Surface Area, Pore Size and Density, pp. 58–81. Springer (2004)

50. Liu, L., Luo, X.-B., Ding, L., Luo, S.-L.: 4-application of nanotechnology in the removal of heavy metal from water. In: Luo, X., Deng, F. (eds.) Nanomaterials for the removal of pollutants and resource reutilization, pp. 83–147. Elsevier, Amsterdam (2019)

51. Patiha, E., Heraldy, Y., Hidayat, M.: Firdaus, The langmuir isotherm adsorption equation: The monolayer approach. IOP Conf. Ser. Mater. Sci. Eng. **107**, 1–9 (2016)

52. Galarneau, A., Villemot, F., Rodriguez, J., Fajula, F., Coasne, B.: Validity of the t-plot Method to Assess Microporosity in Hierarchical Micro/Mesoporous Materials. Langmuir **30**(44), 13266–13274 (2014)

53. Ertl, G., Knözinger, H., Weitkamp, J.: Handbook of heterogeneous catalysis. Wiley (1997)

54. Storck, S., Bretinger, H., Maier, W.F.: Characterization of micro- and mesoporous solids by physisorption methods and pore-size analysis. Appl. Catal. A: Gen. **174**(1), 137–146 (1998)

55. Ali, G.A.M., Supriya, S., Chong, K.F., Shaaban, E.R., Algarni, H., Maiyalagan, T., Hegde, G.: Superior supercapacitance behavior of oxygen self-doped carbon nanospheres: a conversion of Allium cepa peel to energy storage system. Biomass Convers. Biorefin. 1–13 (2019)

56. Ramesh, K., Reddy, K.S., Rashmi, I., Biswas, A.K.: Porosity distribution, surface area, and morphology of synthetic potassium zeolites: A SEM and N2 adsorption study. Commun. Soil Sci. Plant Anal. **45**(16), 2171–2181 (2014)

57. Gauden, P.A., Terzyk, A.P., Rychlicki, G., Kowalczyk, P., Ćwiertnia, M.S., Garbacz, J.K.: Estimating the pore size distribution of activated carbons from adsorption data of different adsorbates by various methods. J. Colloid Interface Sci. **273**(1), 39–63 (2004)

58. Zhu, H.Y., Lu, G.Q., Maes, N., Vansant, E.F.: Pore structure characterisation of pillared clays using a modified MP method. J. Chem. Soc. Faraday Trans. **93**(7), 1417–1423 (1997)

59. Bhat, V.S., Jayeoye, T.J., Rujiralai, T., Sirimahachai, U., Chong, K.F., Hegde, G.: Influence of surface properties on electro-chemical supercapacitors utilizing Callerya atropurpurea pod derived porous nanocarbons: Structure property relationship between porous structures to energy storage devices. Nano Select **1**(2), 226–243 (2020)

60. Supriya, S., Ananthnag, G.S., Shetti, V.S., Nagaraja, B.M., Hegde, G.: Cost-effective bio-derived mesoporous carbon nanoparticles-supported palladium catalyst for nitroarene reduction and Suzuki-Miyaura coupling by microwave approach. Appl. Organomet. Chem. **34**(3), e5384 (2020)

61. Bhat, V.S., Supriya, S., Hegde, G.: Biomass derived carbon materials for electrochemical sensors. J. Electrochem. Soc. **167**(3), 037526 (2019)
62. Akshaya, K.B., Bhat, V.S., Varghese, A., George, L., Hegde, G.: Non-enzymatic electrochemical determination of progesterone using carbon nanospheres from onion peels coated on carbon fiber paper. J. Electrochem. Soc. **166**(13), B1097–B1106 (2019)
63. Bhat, V.S., Hegde, G., Nasrollahzadeh, M.: A sustainable technique to solve growing energy demand: porous carbon nanoparticles as electrode materials for high-performance supercapacitors. J. Appl. Electrochem. **50**, 1243–1255 (2020)
64. Bhat, V.S., Kanagavalli, P., Sriram, G., John, N.S., Veerapandian, M., Kurkuri, M., Hegde, G.: Low cost, catalyst free, high performance supercapacitors based on porous nano carbon derived from agriculture waste. J. Energy Storage **32**, 101829 (2020)
65. Sudhan, N., Subramani, K., Karnan, M., Ilayaraja, N., Sathish, M.: Biomass-derived activated porous carbon from rice straw for a high-energy symmetric supercapacitor in aqueous and non-aqueous electrolytes. Energ. Fuel. **31**(1), 977–985 (2017)

Publisher's Note Springer Nature remains neutral with regard to jurisdictional claims in published maps and institutional affiliations.